Supporting Information for "Modeling global carbon and water fluxes and hyperspectral canopy radiative transfer simultaneously using a next generation land surface model—CliMA Land"

Contents of this file

1. Note S1
2. Table S1
3. Figures S1

Introduction

Note S1 describes the method we used to invert hyperspectral soil albedo from known broadband PAR and NIR albedo values.

Figures S1 and S2 plot the comparison of soil water time series from ERA5 reanalysis data and flux tower observations at AU-Tum (site h of Figure 2 in the main text).

Note S1. Hyperspectral soil albedo

Firstly, to derive hyperspectral soil albedo, we calculate soil albedo values at photosynthetically active radiation (PAR) region and near infrared (NIR) regions, denoted as α_{PAR} and α_{NIR} respectively, by linearly interpolating the reference values at completely wet and dry soils:

$$\alpha_{\text{PAR}} = \alpha_{\text{PAR,wet}} \cdot \text{RSWC} + \alpha_{\text{PAR,dry}} \cdot (1 - \text{RSWC}), \tag{1}$$

$$\alpha_{\text{NIR}} = \alpha_{\text{NIR,wet}} \cdot \text{RSWC} + \alpha_{\text{NIR,dry}} \cdot (1 - \text{RSWC}), \tag{2}$$

where RSWC is the relative volumetric soil water content (0 when completely dry, 1 when soil water content is saturated), the subscript "wet" denotes saturated soil, and the subscript "dry" denotes completely dry soil. The four reference albedo values at a RSWC = 0 and RSWC = 1 can be found in Community Land Model (Table 3.3 in CLM tech notes version 5). Our adapted method differs from the original CLM approach, which uses

$$\alpha_{\text{PAR}} = \max(\alpha_{\text{PAR,dry}}, \alpha_{\text{PAR,wet}} + 0.11 - 0.4 \cdot \text{SWC}),$$

$$\alpha_{\text{NIR}} = \max(\alpha_{\text{NIR,dry}}, \alpha_{\text{NIR,wet}} + 0.11 - 0.4 \cdot \text{SWC}),$$

where SWC is the absolute volumetric soil water content (0 when completely dry, < 1 when saturated). Our adapted soil albedo method linearly interpolates the soil albedo from wet to dry soil, and better matches experimental observations than the original CLM approach (Figure S1.1).

Secondly, we expand the broadband albedo values to hyperspectral by weighing the characteristic soil albedo bands:

$$\alpha(\lambda) = \sum_i f(i) \cdot A(i, \lambda), \tag{3}$$

where $\alpha(\lambda)$ is the albedo at wavelength λ, $f(i)$ is the weight of the ith characteristic albedo band, and $A(i, \lambda)$ is the ith characteristic albedo band. See Figure S1.2 for the four bands.

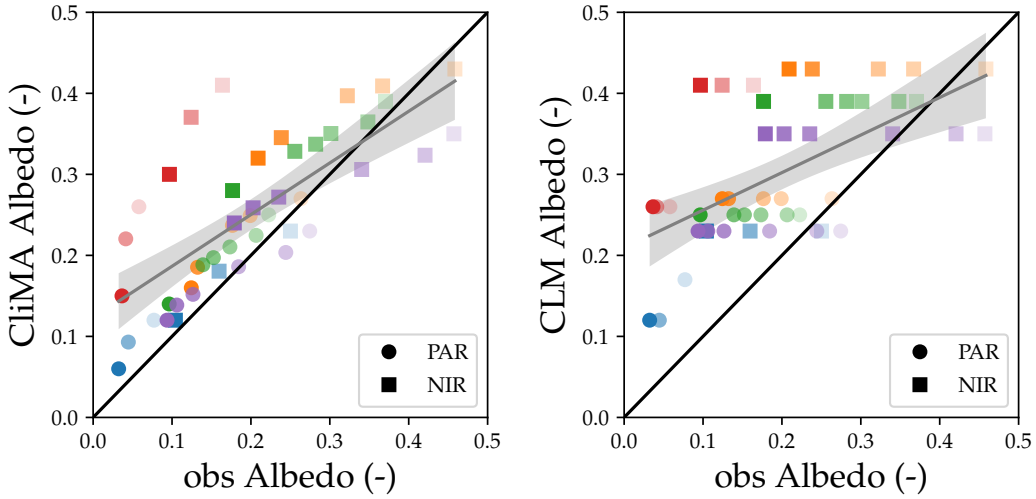

Figure S1.1. Comparison of the broadband albedo computed using the CliMA Land and CLM approach. Data from (Jiang & Fang, 2019).

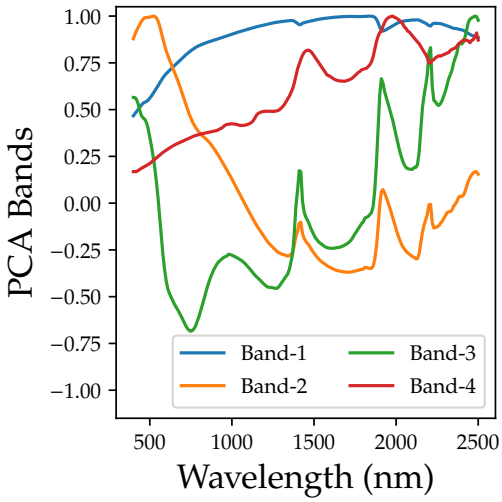

Figure S1.2. Characteristic soil albedo bands of the GSV model (Jiang & Fang, 2019).

We use six methods to fit the weights: three methods using only first two characteristic bands (two fitted weights) and three methods using all four characteristic bands (four fitted weighted). Each of the categories contains (1) point method that fits averages, (2) curve method that fit curves, and (3) hybrid method that fits a point and a curve. The six methods are labeled as 2P, 2C, 2H, 4P, 4C, and 4H, respectively. The point method weighs the PAR and NIR region

equally, and minimizes the sum of the square error between the averages:

$$\min \left[(\overline{\alpha_{\mathrm{PAR,mod}}} - \alpha_{\mathrm{PAR,ref}})^2 + (\overline{\alpha_{\mathrm{NIR,mod}}} - \alpha_{\mathrm{NIR,ref}})^2 \right]. \tag{4}$$

The curve method assumes the target is a two-piece flat curve that the PAR region is constant at $\alpha_{\mathrm{PAR,ref}}$ and the NIR region is constant at $\alpha_{\mathrm{NIR,ref}}$, and minimizes the square error between modeled and target curves:

$$\min \overline{(\alpha_{\mathrm{mod}} - \alpha_{\mathrm{ref}})^2}. \tag{5}$$

The hybrid method weighs the PAR and NIR regions equally, and minimizes the sum of (1) the square error between the averages in the PAR region and (2) square of mean absolute difference between modeled and target curve in the NIR region:

$$\min \left[(\overline{\alpha_{\mathrm{PAR,mod}}} - \alpha_{\mathrm{PAR,ref}})^2 + \left(\overline{|\alpha_{\mathrm{NIR,mod}} - \alpha_{\mathrm{NIR,ref}}|} \right)^2 \right]. \tag{6}$$

See Figure S1.3 for the examples of the fitting methods. Overall, 4H performs the best (Figure S1.4), and we use it in our CliMA Land simulations. Note here that method 4P fits 4 values from 2 albedo so that it does not converge. As a result, method 4P has extremely high error compared to others.

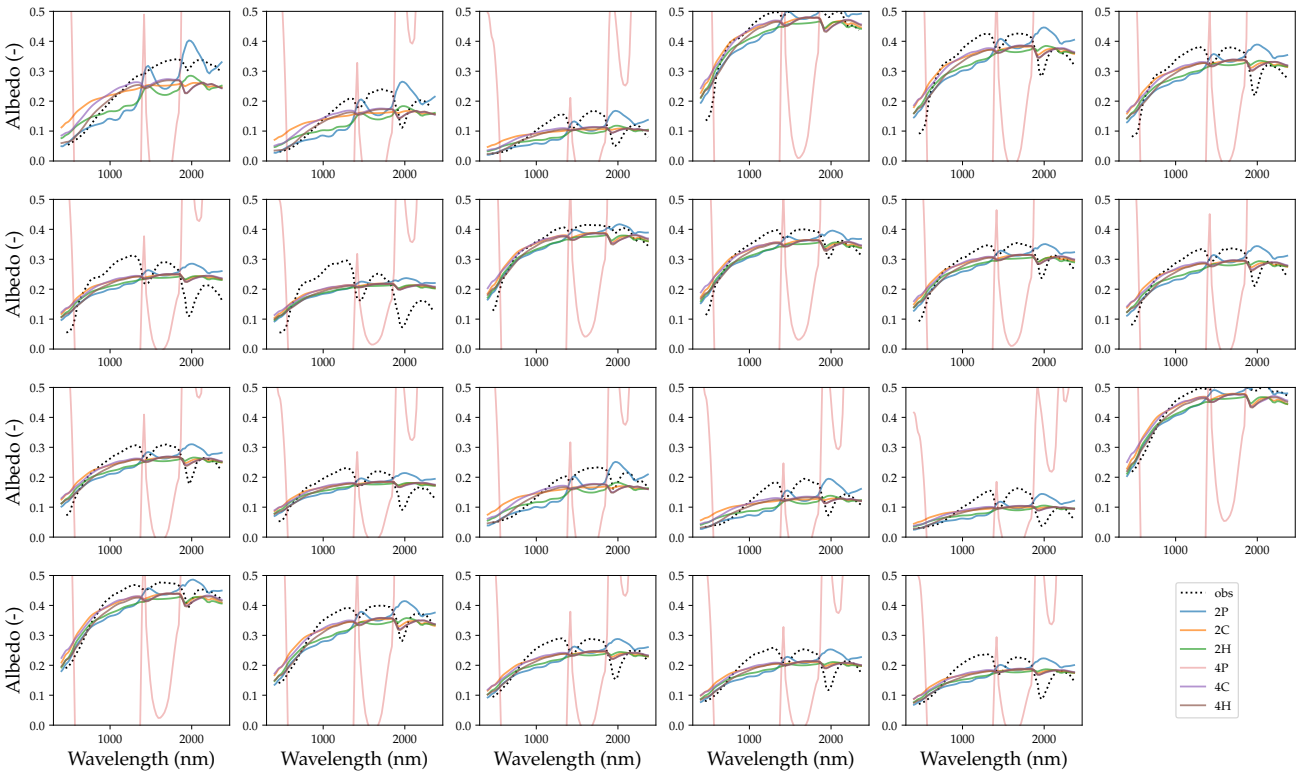

Figure S1.3. Examples of the performances of the six fitting methods. Data from (Jiang & Fang, 2019).

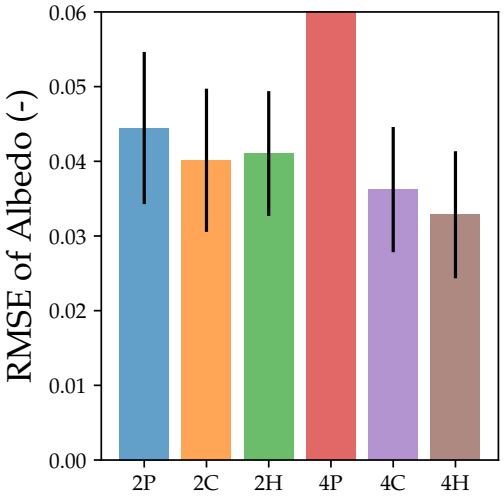

Figure S1.4. Performances of the six fitting methods. Data from (Jiang & Fang, 2019).

Table S1. Coupled Model Intercomparison Project (CMIP) models used for benchmarking.

CMIP5 Model	Reference	CMIP6 Model	Reference
ACCESS1-3	(Lewis & Karoly, 2014)	ACCESS-ESM1-5	(Ziehn et al., 2019)
		BCC-CSM2-MR	(Wu et al., 2018)
CanESM2	(Chylek et al., 2011)	CanESM5	(Swart et al., 2019)
		CESM2	(Danabasoglu, 2019)
		CNRM-ESM2-1	(Seferian, 2018)
GFDL-ESM2M	(GFDL, 2014)	GFDL-ESM4	(Horowitz et al., 2018)
		GISS-E2-1-G	(NASA GISS, 2018)
HadGEM2-CC	(Jones et al., 2011)		
IPSL-CM5A-LR	(Dufresne et al., 2013)	IPSL-CM6A-LR	(Boucher et al., 2018)
MIROC-ESM	(Watanabe et al., 2011)	MIROC-ES2L	(Tachiiri et al., 2019)
MPI-ESM-LR	(Giorgetta et al., 2013)	MPI-ESM1-2-LR	(Wieners et al., 2019)
NorESM1-M	(NCC, 2011)	NorESM2-LM	(Seland et al., 2019)
		UKESM1-0-LL	(Tang et al., 2019)

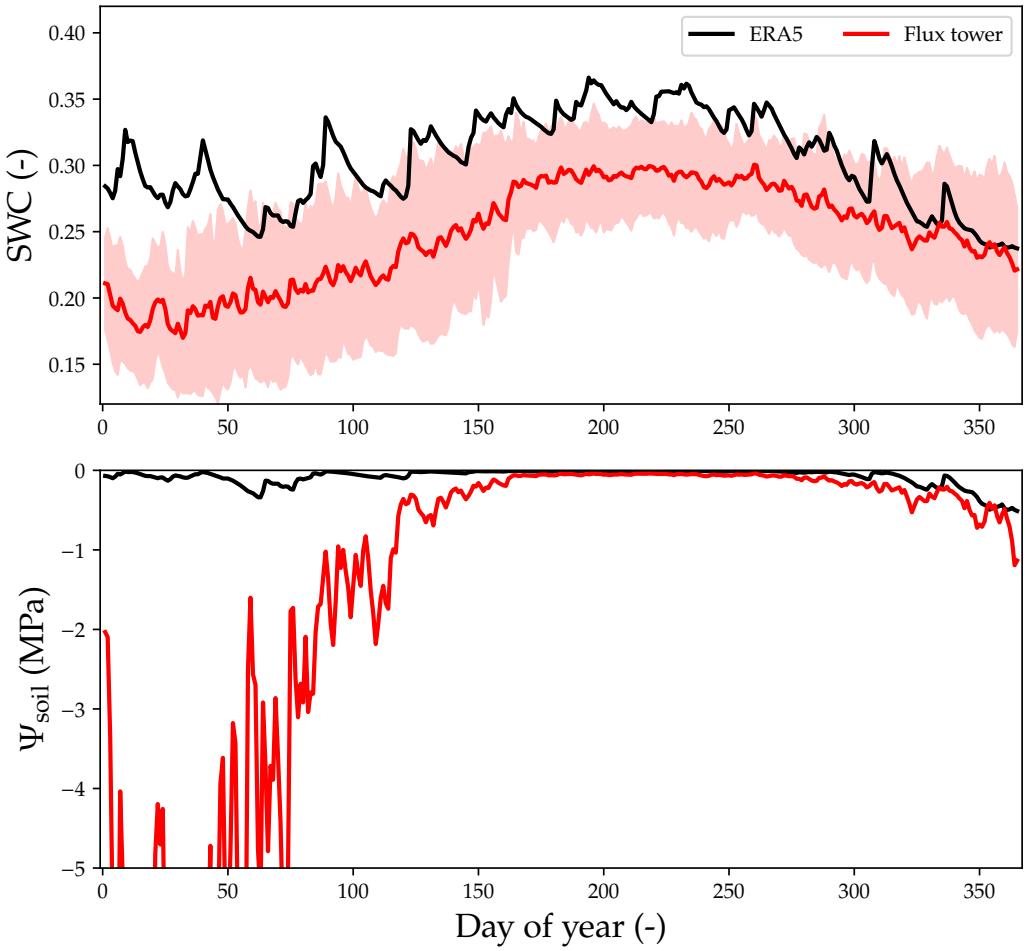

Figure S1. Comparison of soil water time series from ERA5 reanalysis data and flux tower observations at AU-Tum (site h of Figure 2 in the main text). Soil water content (SWC) from ERA5 is averaged from that of four soil layers (black curve), and SWC from flux tower is averaged from that of the same day from year 2001 to 2014 (shaded red region indicates the standard deviation, SD). Soil water potential (Ψ_{soil}) is computed from corresponding SWC using the van Genuchten equation (van Genuchten, 1980) using the gridded soil hydraulic parameters from Dai et al. (2019) for the site. Red region plots the Ψ_{soil} with SWC in the range of mean ± SD.

References

Boucher, O., Denvil, S., Levavasseur, G., Cozic, A., Caubel, A., Foujols, M.-A., ... Cheruy, F. (2018). *Ipsl ipsl-cm6a-lr model output prepared for cmip6 cmip.* Earth System Grid Federation. doi: 10.22033/ESGF/CMIP6.1534

Chylek, P., Li, J., Dubey, M., Wang, M., & Lesins, G. (2011). Observed and model simulated 20th century arctic temperature variability: Canadian earth system model canesm2. *Atmospheric Chemistry and Physics Discussions*, *11*(8), 22893–22907.

Dai, Y., Xin, Q., Wei, N., Zhang, Y., Shangguan, W., Yuan, H., ... Lu, X. (2019). A global high-resolution data set of soil hydraulic and thermal properties for land surface modeling. *Journal of Advances in Modeling Earth Systems*, *11*(9), 2996–3023.

Danabasoglu, G. (2019). *Ncar cesm2 model output prepared for cmip6 cmip historical.* Earth System Grid Federation. doi: 10.22033/ESGF/CMIP6.7627

Dufresne, J.-L., Foujols, M.-A., Denvil, S., Caubel, A., Marti, O., Aumont, O., ... Vuichard, N. (2013). Climate change projections using the ipsl-cm5 earth system model: from cmip3 to cmip5. *Climate dynamics*, *40*(9), 2123–2165.

GFDL. (2014). *Noaa gfdl gfdl-esm2m, historicalmisc experiment output for cmip5 ar5, served by esgf.* World Data Center for Climate (WDCC) at DKRZ. doi: 10.1594/WDCC/CMIP5.NGEMhm

Giorgetta, M. A., Jungclaus, J., Reick, C. H., Legutke, S., Bader, J., Böttinger, M., ... Stevens, B. (2013). Climate and carbon cycle changes from 1850 to 2100 in mpi-esm simulations for the coupled model intercomparison project phase 5. *Journal of Advances in Modeling Earth Systems*, *5*(3), 572–597.

Horowitz, L. W., Naik, V., Sentman, L., Paulot, F., Blanton, C., McHugh, C., ... Zeng, Y.

(2018). *Noaa-gfdl gfdl-esm4 model output prepared for cmip6 aerchemmip.* Earth System Grid Federation. doi: 10.22033/ESGF/CMIP6.1404

Jiang, C., & Fang, H. (2019). Gsv: a general model for hyperspectral soil reflectance simulation. *International Journal of Applied Earth Observation and Geoinformation*, *83*, 101932.

Jones, C. D., Hughes, J. K., Bellouin, N., Hardiman, S. C., Jones, G. S., Knight, J., ... Zerroukat, M. (2011). The hadgem2-es implementation of cmip5 centennial simulations. *Geoscientific Model Development*, *4*(3), 543–570.

Lewis, S. C., & Karoly, D. J. (2014). Assessment of forced responses of the australian community climate and earth system simulator (access) 1.3 in cmip5 historical detection and attribution experiments. *AUSTRALIAN BUREAU METEOROLOGY*.

NASA GISS. (2018). *Nasa-giss giss-e2.1g model output prepared for cmip6 ismip6.* Earth System Grid Federation. doi: 10.22033/ESGF/CMIP6.2066

NCC. (2011). *Noresm1-m model output prepared for cmip5, served by esgf.* World Data Center for Climate (WDCC) at DKRZ.

Seferian, R. (2018). *Cnrm-cerfacs cnrm-esm2-1 model output prepared for cmip6 cmip.* Earth System Grid Federation. doi: 10.22033/ESGF/CMIP6.1391

Seland, Ø., Bentsen, M., Oliviè, D. J. L., Toniazzo, T., Gjermundsen, A., Graff, L. S., ... Schulz, M. (2019). *Ncc noresm2-lm model output prepared for cmip6 cmip historical.* Earth System Grid Federation. doi: 10.22033/ESGF/CMIP6.8036

Swart, N. C., Cole, J. N., Kharin, V. V., Lazare, M., Scinocca, J. F., Gillett, N. P., ... Sigmond, M. (2019). *Cccma canesm5 model output prepared for cmip6 scenariomip.* Earth System Grid Federation. doi: 10.22033/ESGF/CMIP6.1317

Tachiiri, K., Abe, M., Hajima, T., Arakawa, O., Suzuki, T., Komuro, Y., ... Kawamiya, M.

(2019). *Miroc miroc-es2l model output prepared for cmip6 scenariomip.* Earth System Grid Federation. doi: 10.22033/ESGF/CMIP6.936

Tang, Y., Rumbold, S., Ellis, R., Kelley, D., Mulcahy, J., Sellar, A., ... Jones, C. (2019). *Mohc ukesm1.0-ll model output prepared for cmip6 cmip historical.* Earth System Grid Federation. doi: 10.22033/ESGF/CMIP6.6113

van Genuchten, M. T. (1980). A closed-form equation for predicting the hydraulic conductivity of unsaturated soils. *Soil science society of America journal*, *44*(5), 892–898.

Watanabe, S., Hajima, T., Sudo, K., Nagashima, T., Takemura, T., Okajima, H., ... Kawamiya, M. (2011). Miroc-esm 2010: model description and basic results of cmip5-20c3m experiments. *Geoscientific Model Development*, *4*(4), 845–872.

Wieners, K.-H., Giorgetta, M., Jungclaus, J., Reick, C., Esch, M., Bittner, M., ... Roeckner, E. (2019). *Mpi-m mpi-esm1.2-lr model output prepared for cmip6 scenariomip ssp245.* Earth System Grid Federation. doi: 10.22033/ESGF/CMIP6.6693

Wu, T., Chu, M., Dong, M., Fang, Y., Jie, W., Li, J., ... Zhang, Y. (2018). *Bcc bcc-csm2mr model output prepared for cmip6 cmip picontrol.* Earth System Grid Federation. doi: 10.22033/ESGF/CMIP6.3016

Ziehn, T., Chamberlain, M., Lenton, A., Law, R., Bodman, R., Dix, M., ... Druken, K. (2019). *Csiro access-esm1.5 model output prepared for cmip6 cmip.* Earth System Grid Federation. doi: 10.22033/ESGF/CMIP6.2288